Search for $K_L \to \pi^0 \nu \bar{\nu}$ and $K_L \to \pi^0 X^0$ Decays at the J-PARC KOTO Experiment

J. K. Ahn,[1] B. Beckford,[2] J. Beechert,[2] K. Bryant,[2] M. Campbell,[2] S. H. Chen,[3] J. Comfort,[4] K. Dona,[2] N. Hara,[5] H. Haraguchi,[5] Y. B. Hsiung,[3] M. Hutcheson,[2] T. Inagaki,[6] I. Kamiji,[7] N. Kawasaki,[7] E. J. Kim,[8] J. L. Kim,[1,†] Y. J. Kim,[9] J. W. Ko,[9] T. K. Komatsubara,[6,10] K. Kotera,[5] A. S. Kurilin,[11,*] J. W. Lee,[5,‡] G. Y. Lim,[6,10] C. Lin,[3] Q. Lin,[12] Y. Luo,[12] J. Ma,[12] Y. Maeda,[7,§] T. Mari,[5] T. Masuda,[7,‖] T. Matsumura,[13] D. Mcfarland,[4] N. McNeal,[2] J. Micallef,[2] K. Miyazaki,[5] R. Murayama,[5,¶] D. Naito,[7,¶] K. Nakagiri,[7] H. Nanjo,[7,**] H. Nishimiya,[5] T. Nomura,[6,10] M. Ohsugi,[5] H. Okuno,[6] M. Sasaki,[14] N. Sasao,[15] K. Sato,[5,††] T. Sato,[6] Y. Sato,[5] H. Schamis,[2] S. Seki,[7] N. Shimizu,[5] T. Shimogawa,[16,¶] T. Shinkawa,[13] S. Shinohara,[7] K. Shiomi,[6,10] S. Su,[2] Y. Sugiyama,[5,¶] S. Suzuki,[16] Y. Tajima,[14] M. Taylor,[2] M. Tecchio,[2] M. Togawa,[5,¶] Y. C. Tung,[12] Y. W. Wah,[12] H. Watanabe,[6,10] J. K. Woo,[9] T. Yamanaka,[5] and H. Y. Yoshida[14]

(KOTO Collaboration)

[1]*Department of Physics, Korea University, Seoul 02841, Republic of Korea*
[2]*Department of Physics, University of Michigan, Ann Arbor, Michigan 48109, USA*
[3]*Department of Physics, National Taiwan University, Taipei, Taiwan 10617, Republic of China*
[4]*Department of Physics, Arizona State University, Tempe, Arizona 85287, USA*
[5]*Department of Physics, Osaka University, Toyonaka, Osaka 560-0043, Japan*
[6]*Institute of Particle and Nuclear Studies, High Energy Accelerator Research Organization (KEK), Tsukuba, Ibaraki 305-0801, Japan*
[7]*Department of Physics, Kyoto University, Kyoto 606-8502, Japan*
[8]*Division of Science Education, Chonbuk National University, Jeonju 54896, Republic of Korea*
[9]*Department of Physics, Jeju National University, Jeju 63243, Republic of Korea*
[10]*J-PARC Center, Tokai, Ibaraki 319-1195, Japan*
[11]*Laboratory of Nuclear Problems, Joint Institute for Nuclear Researches, Dubna, Moscow region 141980, Russia*
[12]*Enrico Fermi Institute, University of Chicago, Chicago, Illinois 60637, USA*
[13]*Department of Applied Physics, National Defense Academy, Kanagawa 239-8686, Japan*
[14]*Department of Physics, Yamagata University, Yamagata 990-8560, Japan*
[15]*Research Institute for Interdisciplinary Science, Okayama University, Okayama 700-8530, Japan*
[16]*Department of Physics, Saga University, Saga 840-8502, Japan*

A search for the rare decay $K_L \to \pi^0 \nu \bar{\nu}$ was performed. With the data collected in 2015, corresponding to 2.2×10^{19} protons on target, a single event sensitivity of $(1.30 \pm 0.01_{\text{stat}} \pm 0.14_{\text{syst}}) \times 10^{-9}$ was achieved and no candidate events were observed. We set an upper limit of 3.0×10^{-9} for the branching fraction of $K_L \to \pi^0 \nu \bar{\nu}$ at the 90% confidence level (C.L.), which improved the previous limit by almost an order of magnitude. An upper limit for $K_L \to \pi^0 X^0$ was also set as 2.4×10^{-9} at the 90% C.L., where X^0 is an invisible boson with a mass of 135 MeV/c^2.

Introduction.—The $K_L \to \pi^0 \nu \bar{\nu}$ decay is a *CP*-violating process and is highly suppressed in the standard model (SM) due to the $s \to d$ flavor-changing neutral current transition [1,2]. The branching fraction for this decay can be accurately calculated, and is one of the most sensitive probes to search for new physics beyond the SM (see, e.g., Refs. [3–10]). The SM prediction is $(3.00 \pm 0.30) \times 10^{-11}$

[11], while the best upper limit was 2.6×10^{-8} (90% C.L.) [12] set by the KEK E391a experiment [13]. An indirect upper limit, called the Grossman-Nir bound [14], of 1.46×10^{-9} is based on the $K^+ \to \pi^+ \nu \bar{\nu}$ measurement by the BNL E949 experiment [15].

The KOTO experiment [16,17] at the Japan Proton Accelerator Research Complex (J-PARC) [18] is dedicated to studying the $K_L \to \pi^0 \nu \bar{\nu}$ decay. The first physics run was conducted in 2013 and achieved a comparable sensitivity to E391a with 100 h of data taking [19]. KOTO is also sensitive to the $K_L \to \pi^0 X^0$ decay [20,21], where X^0 is an invisible light boson. The upper limit for this decay was set, for the first time in Ref. [19], as 3.7×10^{-8} (90% C.L.) for the X^0 mass of 135 MeV/c^2.

Experimental methods and apparatus.—A 30-GeV proton beam extracted from the J-PARC Main Ring accelerator with a duration of 2 s struck a gold production target [22], and secondary neutral particles produced at an angle of 16° from the proton beam were transported via the "KL beam line" [23] to the experimental area. The neutral beam, composed of neutrons, photons, and K_L's, was collimated by two collimators made of iron and tungsten to a size of 8×8 cm^2 by the end of the 20-m-long beam line. The peak K_L momentum was 1.4 GeV/c, and the K_L flux was measured [24,25] as 4.2×10^7 K_L's per 2×10^{14} protons on the target at the exit of the beam line. The neutron (kinetic energy > 100 MeV) and photon (energy > 10 MeV) fluxes were estimated to be 6 and 7 times larger than the kaon, respectively. Neutrons scattered by the collimators outside the nominal solid angle of the beam are referred to as "halo neutrons." The collimators were aligned with a beam profile monitor [26] to minimize the halo neutrons.

A schematic view of the KOTO detector is shown in Fig. 1. The origin of the z axis which lies along the beam direction was the upstream edge of FB, 21.5 m away from the target. The x (horizontal) and y (vertical) axes were defined as in the right-handed coordinate system. The KOTO detector consisted of the CsI calorimeter (CSI) and hermetic veto counters around the decay volume in vacuum. The signature of the $K_L \rightarrow \pi^0 \nu \bar{\nu}$ decay was "two photons + nothing else"; we measured two photons from a π^0 decay with CSI and ensured that there were no other detectable particles in CSI and veto counters. The CSI was composed of 2716 undoped CsI crystals whose length was 50 cm and cross section was 2.5×2.5 cm^2 (5×5 cm^2) within (outside) the central 1.2×1.2 m^2 region. The 15×15 cm^2 region at the center of CSI was the beam hole to let the beam particles pass through. The veto counters consisted of lead-scintillator sandwich, lead-aerogel, or undoped-CsI counters for photons and plastic scintillators or wire chambers for charged particles. The waveform of the signal from all of the detector components was recorded with either 125-MHz digitizers after a Gaussian shaper

circuitry [27] or 500-MHz digitizers [28]. Details of the detector components and new components after the 2013 run are explained in Refs. [17,19,29].

Data taking.—This Letter is based on the data set collected in 2015 corresponding to 2.2×10^{19} protons on target. The power of the primary proton beam increased from 24 to 42 kW during the period. The K_L rate at the exit of the beam line was 10 MHz. The data acquisition system was triggered by two stages of trigger logic [30,31]. The first-level trigger (L1) required energy deposition larger than 550 MeV in CSI and the absence of energy deposition in four veto counters which surrounded the decay volume (MB, CV, NCC, and CC03 in Fig. 1) using loose veto criteria. The second-level trigger (L2) calculated the center of energy deposition (COE) in CSI and required the distance from the beam center (R_{COE}) to be larger than 165 mm. L2 was implemented to reduce the contamination of the $K_L \rightarrow 3\pi^0$ decay with small missing energy. We collected 4.31×10^9 events for the signal sample with these trigger requirements. We simultaneously collected samples of $K_L \rightarrow 3\pi^0$, $K_L \rightarrow 2\pi^0$, and $K_L \rightarrow 2\gamma$ decays for the purpose of normalization and calibration by disregarding the L2 decision (and without veto requirements in the L1 decision) with a prescaling factor of 30 (300).

Reconstruction and event selection.—The electromagnetic shower generated by a photon in CSI was reconstructed using a cluster of hits in adjacent crystals with energies larger than 3 MeV. A π^0 was reconstructed from two clusters in CSI assuming the $\pi^0 \rightarrow 2\gamma$ decay. The opening angle θ of the two photons was calculated with $\cos \theta = 1 - M_{\pi^0}^2 / (2E_{\gamma_1} E_{\gamma_2})$, where M_{π^0} is the nominal π^0 mass, and E_{γ_1} and E_{γ_2} are the energies of two photons. The π^0 decay vertex (Z_{vtx}) and transverse momentum (P_t) were calculated assuming that the vertex was on the beam axis. In the case of the $K_L \rightarrow \pi^0 \nu \bar{\nu}$ decay, the reconstructed π^0 should have a finite P_t due to the two missing neutrinos. Signal candidates were required to have Z_{vtx} in the range of $3000 < Z_{vtx} < 4700$ mm to avoid π^0's generated by halo neutrons hitting detector components. The K_L decay probability in the Z_{vtx} range was 3.2%. The candidates
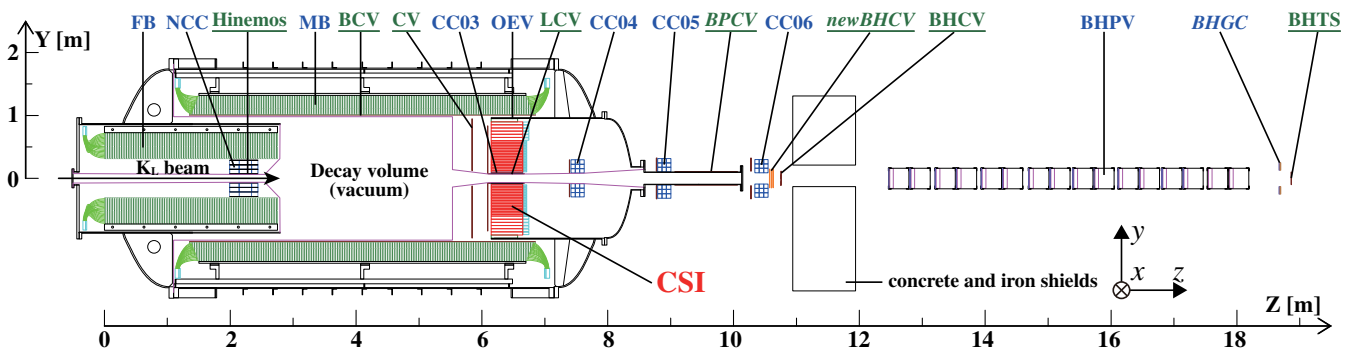

FIG. 1. Cross-sectional view of the KOTO detector. The beam enters from the left. Detector components with their abbreviated names written in blue (in green and underlined) are photon (charged particle) veto counters. BPCV, newBHCV, and BHGC are new counters installed after 2013. BHCV and BHTS were not used in the analysis.

were also required to have a P_t in the range of $P_t^{\min}(Z_{\rm vtx}) < P_t < 250$ MeV/c, where $P_t^{\min}(Z_{\rm vtx})$ was 130 MeV/c in the range of $3000 < Z_{\rm vtx} < 4000$ mm and varied linearly from 130 to 150 MeV/c in the range of $4000 < Z_{\rm vtx} < 4700$ mm. This requirement on P_t greatly suppressed events from the $K_L \to \pi^+\pi^-\pi^0$ decay.

A series of selection criteria (cuts) based on the energy, timing, and position of the two clusters in CSI were imposed on the candidates. We determined all the cuts without examining events inside the region $2900 < Z_{\rm vtx} < 5100$ mm and $120 < P_t < 260$ MeV/c. In order to ensure the consistency with trigger conditions, we required $E_{\gamma_1} + E_{\gamma_2} > 650$ MeV and $R_{\rm COE} > 200$ mm (trigger-related cuts). For each reconstructed photon, we required $100 < E_\gamma < 2000$ MeV and the hit position (x, y) to be in the CSI fiducial region of $\sqrt{x^2 + y^2} < 850$ mm and $\min(|x|, |y|) > 150$ mm (photon selection cuts). The following kinematic cuts on the two photons in CSI were imposed. Consistency of the timing of two photons, after taking into account the time of flight from the π^0 decay vertex to CSI, was required to be within 1 ns of each other. The distance between the two clusters was required to be larger than 300 mm to ensure a clean separation. To avoid mismeasurement of photon energies due to three dead channels in CSI, the position of clusters was required to be more than 53 mm apart from those channels. The ratio of the energy of two photons, $E_{\gamma_2}/E_{\gamma_1}$ $(E_{\gamma_1} > E_{\gamma_2})$, was required to be larger than 0.2 to reduce a class of the $K_L \to 2\pi^0$ background originating from miscombinations of two photons in the π^0 reconstruction. For the same purpose, the product of the energy and the angle between the beam axis and the momentum of a photon was required to be larger than 2500 MeV deg. The opening angle of two photons in the x-y plane was required to be smaller than 150° to reduce the $K_L \to 2\gamma$ background, in which the photons are back to back. To select π^0 candidates with plausible kinematics, allowed regions were set on $P_t/P_z - Z_{\rm vtx}$ and $E - Z_{\rm vtx}$ planes, where P_z and E are the longitudinal momentum and energy of the π^0, respectively. This cut was effective in reducing the "CV-η background," which is described later. Events were rejected if there were any hits in the veto counters coincident with the π^0 decay. Cluster-shape and pulse-shape cuts in the CSI (shape-related cuts), defined later, were also imposed on the photons from π^0 candidates to reduce the background from photon-cluster fusion and neutron showers.

The signal acceptance $A_{\rm sig}$ was evaluated using GEANT4-based [32–34] Monte Carlo (MC) simulations. Accidental activities in the KOTO detector were taken into account by overlaying random trigger data collected during the data taking. The $A_{\rm sig}$ was calculated at 0.52% after convoluting the reduction from kinematic (57%), veto (17%), and shape-related (52%) cuts. The data reduction is summarized in Table I.

TABLE I. Data reduction in each of the selection criteria.

Selection criteria	No. events
Triggered events	4.31×10^9
Two clusters	8.74×10^8
Trigger-related cuts	2.50×10^8
Photon selection cuts	1.75×10^8
Kinematic cuts	3.59×10^7
Veto cuts	3.83×10^4
Shape-related cuts	347

Normalization and single event sensitivity (SES).—The sensitivity for the signal was normalized to the $K_L \to 2\pi^0$ decay; events with four photons in CSI were used to reconstruct the $K_L \to 2\pi^0$ events by requiring the pair of π^0's with the smallest $Z_{\rm vtx}$ difference among all possible combinations of four photons, together with a series of kinematic and extra-particle veto cuts. The weighted mean of the two $Z_{\rm vtx}$'s was used to define the decay vertex and select $K_L \to 2\pi^0$ events within the same decay region as the signal. Figure 2 shows the reconstructed K_L mass distribution after imposing all the cuts except for the cut on the K_L mass; events within ± 15 MeV/c^2 around the K_L mass peak were accepted as $K_L \to 2\pi^0$ events.

The single event sensitivity for the $K_L \to \pi^0 \nu \bar{\nu}$ decay was obtained to be

$$\text{SES} = \frac{1}{A_{\rm sig}} \frac{A_{\rm norm} \text{Br}(K_L \to 2\pi^0)}{p N_{\rm norm}}, \tag{1}$$

where $A_{\rm norm}$ is the acceptance for $K_L \to 2\pi^0$ evaluated based on MC simulations, $\text{Br}(K_L \to 2\pi^0)$ is the branching fraction of $K_L \to 2\pi^0$ [12], p is the prescale factor of 30 used to collect the $K_L \to 2\pi^0$ sample, and $N_{\rm norm}$ is the number of reconstructed $K_L \to 2\pi^0$ events in the data after
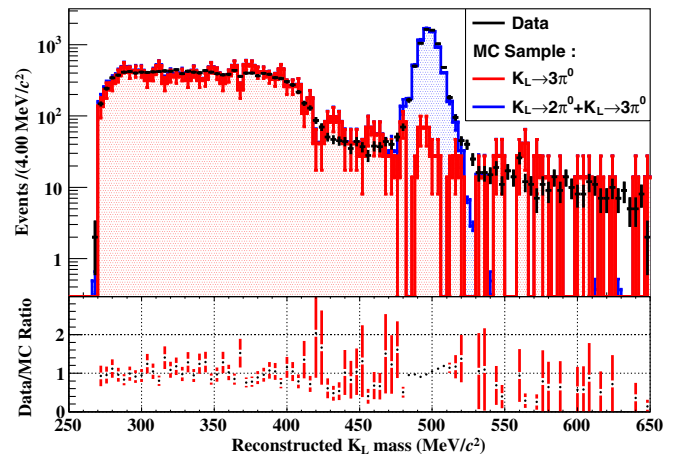

FIG. 2. Four-photon invariant mass distribution of the $K_L \to 2\pi^0$ events after imposing all the cuts except for the K_L mass cut. The bottom panel shows the ratio of data and MC (sum of $K_L \to 2\pi^0$ and $K_L \to 3\pi^0$) for each histogram bin.

TABLE II. Summary of relative systematic uncertainties in the single event sensitivity.

Source	Uncertainty [%]
Trigger effect	1.9
Photon selection cuts	0.81
Kinematic cuts for $K_L \to \pi^0 \nu \bar{\nu}$	5.1
Veto cuts	3.7
Shape-related cuts	5.1
K_L momentum spectrum	1.1
Kinematic cuts for $K_L \to 2\pi^0$	2.7
$K_L \to 2\pi^0$ branching fraction	0.69
Normalization modes inconsistency	5.6
Total	11

TABLE III. Summary of background estimation.

Source		No. events
K_L decay	$K_L \to \pi^+ \pi^- \pi^0$	0.05 ± 0.02
	$K_L \to 2\pi^0$	0.02 ± 0.02
	Other K_L decays	0.03 ± 0.01
Neutron induced	Hadron cluster	0.24 ± 0.17
	Upstream π^0	0.04 ± 0.03
	CV η	0.04 ± 0.02
Total		0.42 ± 0.18

subtracting the $K_L \to 3\pi^0$ contamination. Based on $A_{\text{norm}} = 0.36\%$ and $N_{\text{norm}} = 1.52 \times 10^4$, the SES was evaluated to be $(1.30 \pm 0.01_{\text{stat}} \pm 0.14_{\text{syst}}) \times 10^{-9}$. The sensitivity is almost an order of magnitude better compared to that of E391a [13] and KOTO's first results [19], and comparable to the Grossman-Nir bound. The expected number of the SM signal events is 0.023 in this analysis.

The systematic uncertainties in the SES are summarized in Table II. The major sources of the uncertainty were the kinematic cuts for the $K_L \to \pi^0 \nu \bar{\nu}$ selection, the shape-related cuts, and the consistency among the normalization decays $K_L \to 2\pi^0$, $K_L \to 3\pi^0$, and $K_L \to 2\gamma$. The former two were evaluated as follows. A sample of π^0's from the reconstructed $K_L \to 2\pi^0$ events was used as a validation sample. The discrepancy between data and MC acceptance, defined as $(A_{\text{MC}}^i - A_{\text{data}}^i)/A_{\text{data}}^i$, where $A_{\text{data(MC)}}^i$ represents the acceptance of the ith cut for data (MC), was used to estimate the systematic uncertainty of the ith cut. The sum in quadrature of the uncertainties for each of the kinematic cuts and shape-related cuts resulted in a total systematic uncertainty of 5.1% for both sets, as shown in Table II. The sensitivity was measured with the $K_L \to 3\pi^0$ and $K_L \to 2\gamma$ decays, and their difference contributed the single largest source of systematic uncertainties of 5.6%.

Background estimation.—Table III summarizes the background estimation. The total number of estimated background events in the signal region was 0.42 ± 0.18. We categorized background sources into two groups: K_L decay background and neutron-induced background.

The K_L decay background was estimated using MC simulations. The $K_L \to \pi^+ \pi^- \pi^0$ background was due to the absorption of charged pions in the uninstrumented material downstream of CSI. The background from K_L decays was small compared to the neutron-induced background in this analysis.

The neutron-induced background, which was caused by halo neutrons hitting a detector component, was subdivided into the following three categories.

The background called "hadron cluster" [35] was caused by a halo neutron directly hitting CSI and creating a hadronic shower and by a neutron produced in the primary shower to create a second, separated hadronic shower. These two showers mimicked the clusters from $\pi^0 \to 2\gamma$. A data-driven approach was taken to estimate this background. A control sample was collected in special runs with a 10-mm-thick aluminum plate inserted to the beam core at $Z = -634$ mm to scatter neutrons. Two-cluster events were selected in this control sample with selection criteria similar to those used for the signal sample. Two types of cuts were used to reduce the contamination from these neutron-induced events based on cluster-shape discrimination [36] and pulse-shape discrimination [37]. A photonlike cluster was selected by considering several variables based on an electromagnetic shower library produced by the MC simulation. The variable with the most discriminating power between photon and neutron clusters was an energy-based likelihood calculated using the accumulated energy distribution in each crystal as a probability density function. Additional variables, such as global energy and cluster timing information, were used in minimum chi-square estimations and combined with the energy-based likelihood as inputs to a neural network [38] with a single output variable able to distinguish between electromagnetic and hadronic cluster hypotheses. The pulse-shape discrimination used the waveform of readout signal from each CSI crystal. The waveform was fitted to the following asymmetric Gaussian:

$$A(t) = |A| \exp\left(-\frac{(t-t_0)^2}{2\sigma(t)^2}\right), \quad (2)$$

where $\sigma(t) = \sigma_0 + a(t - t_0)$ depends on the timing difference from the mean of the Gaussian (t_0). Using templates of the fit parameters, σ_0 and a, obtained in a hadron-cluster control sample and by a photon sample from $K_L \to 3\pi^0$, a likelihood ratio was calculated to determine whether the clusters are more likely to be the hadron clusters or two photon clusters. We evaluated the rejection power of cuts based on these two discrimination variables for the Al-plate control sample by taking their correlation into account. The number of background events was normalized by comparing the numbers of events of the signal sample and of the control sample outside the signal region before imposing
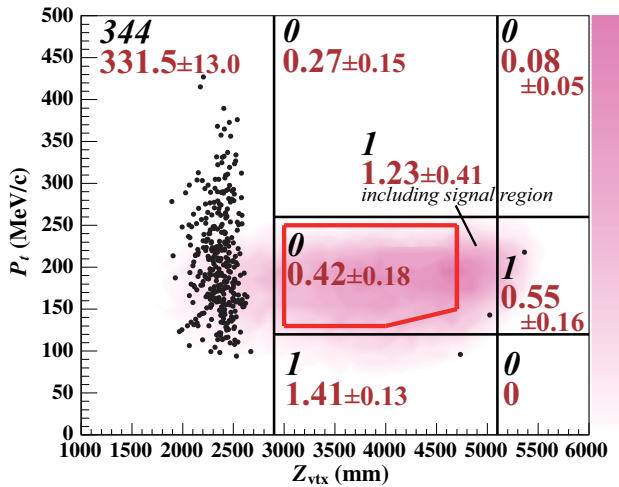
FIG. 3. Reconstructed π^0 transverse momentum (P_t) vs π^0 decay vertex position (Z_{vtx}) plot of the events with all the cuts imposed. The region surrounded by red lines is the signal region. The black dots represent observed events, and the contour indicates the $K_L \to \pi^0 \nu \bar{\nu}$ signal distribution derived from MC simulation. The black italic (red regular) numbers indicate the numbers of observed (expected background) events for the regions inside the lines.

FIG. 4. Upper limit at the 90% C.L. for the $K_L \to \pi^0 X^0$ branching fraction as a function of the X^0 mass. For comparison, the limit for the $K_L \to \pi^0 \nu \bar{\nu}$ decay is shown with the red line.

these cuts, and was estimated to be 0.24. Note that this is an overestimate due to kaon contamination in the control sample, which we were unable to subtract quantitatively from the estimation because of the limited statistics.

The background called "upstream π^0" was caused by halo neutrons hitting the NCC counter in the upstream end of the decay volume and producing π^0's. The reconstructed Z_{vtx} for such decays is shifted downstream into the signal region if the energies of photons are mismeasured to be smaller due to photo-nuclear interactions in CSI, or if one photon in the CSI is paired to a secondary neutron interacting in the CSI to reconstruct the π^0. This background was evaluated by simulation, and the yield was normalized to the number of events in the upstream region in the data and MC calculations. We estimated the number of this background to be 0.04.

The background called "CV η" stemmed from the η production in the halo-neutron interaction with CV [39], which was a veto counter of plastic scintillator for charged particles located in front of CSI. In this background, when a halo neutron hit CV and produced an η meson, and the two photons from the η decay hit CSI, the two clusters were reconstructed using the π^0 mass hypothesis which pushes the reconstructed Z_{vtx} upstream into the signal region. This background was suppressed by imposing a cut which evaluates the consistency of the shape of the clusters with the incident angle of the photons originated from the $\eta \to 2\gamma$ decay produced at CV. The number of the background events was estimated to be 0.04.

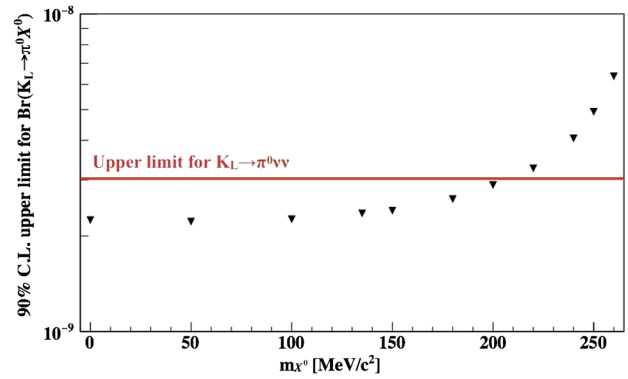*Conclusions and prospects.*—After all the cuts were imposed, no signal candidate events were observed, as shown in Fig. 3. Assuming Poisson statistics with uncertainties taken into account [40], the upper limit for the branching fraction of the $K_L \to \pi^0 \nu \bar{\nu}$ decay was obtained to be 3.0×10^{-9} at the 90% C.L. The upper limit for the $K_L \to \pi^0 X^0$ decay as a function of the X^0 mass (m_{X^0}) was also obtained as shown in Fig. 4; the limit for $m_{X^0} = m_{\pi^0}$ was set to be 2.4×10^{-9} (90% C.L.). These results improve the upper limit of the direct search by almost an order of magnitude.

Based on this analysis, we developed necessary measures to reach better sensitivity. We anticipate to improve background rejection with data collected after 2015, which corresponds to 1.4 times larger than the data in 2015, with a newly added veto counter in 2016 [41] and more refined analysis methodologies, exploiting the substantially higher statistics of the collected control samples.

[*]Deceased.

[†]Present address: Division of Science Education, Chonbuk National University, Jeonju 54896, Republic of Korea.

[‡]Present address: Department of Physics, Korea University, Seoul 02841, Republic of Korea.

[§]Present address: Kobayashi-Maskawa Institute, Nagoya University, Nagoya 464-8602, Japan.

[∥]Present address: Research Institute for Interdisciplinary Science, Okayama University, Okayama 700-8530, Japan.

[¶]Present address: KEK, Tsukuba, Ibaraki 305-0801, Japan.

[**]Present address: Department of Physics, Osaka University, Toyonaka, Osaka 560-0043, Japan.

[††]Present address: Kamioka Observatory, Institute for Cosmic Ray Research, University of Tokyo, Kamioka, Gifu 506-1205, Japan.

[1] L. S. Littenberg, Phys. Rev. D **39**, 3322 (1989).

[2] V. Cirigliano, G. Ecker, H. Neufeld, A. Pich, and J. Portolés, Rev. Mod. Phys. **84**, 399 (2012), and references therein.

[3] A. J. Buras, D. Buttazzo, and R. Knegjens, J. High Energy Phys. 11 (2015) 166.

[4] M. Tanimoto and K. Yamamoto, Prog. Theor. Exp. Phys. **2016**, 123B02 (2016).

[5] A. Crivellin, G. D'Ambrosio, T. Kitahara, and U. Nierste, Phys. Rev. D **96**, 015023 (2017).

[6] M. Bordone, D. Buttazzo, G. Isidori, and J. Monnard, Eur. Phys. J. C **77**, 618 (2017).

[7] S. Fajfer, N. Košnik, and L. V. Silva, Eur. Phys. J. C **78**, 275 (2018).

[8] M. Endo, T. Goto, T. Kitahara, S. Mishima, D. Ueda, and K. Yamamoto, J. High Energy Phys. 04 (2018) 19.

[9] X.-G. He, G. Valencia, and K. Wong, Eur. Phys. J. C **78**, 472 (2018).

[10] C.-H. Chen and T. Nomura, J. High Energy Phys. 08 (2018) 145.

[11] A. J. Buras, D. Buttazzo, J. Girrbach-Noe, and R. Knegjens, J. High Energy Phys. 11 (2015) 33.

[12] M. Tanabashi et al. (Particle Data Group), Phys. Rev. D **98**, 030001 (2018).

[13] J. K. Ahn et al. (E391a Collaboration), Phys. Rev. D **81**, 072004 (2010).

[14] Y. Grossman and Y. Nir, Phys. Lett. B **398**, 163 (1997).

[15] A. V. Artamonov et al. (E949 Collaboration), Phys. Rev. D **79**, 092004 (2009).

[16] J. Comfort et al., Proposal for $K_L \to \pi^0 \nu \bar{\nu}$ experiment at J-Parc, 2006, https://j-parc.jp/researcher/Hadron/en/pac_0606/pdf/p14-Yamanaka.pdf.

[17] T. Yamanaka, Prog. Theor. Exp. Phys. **2012**, 02B006 (2012).

[18] S. Nagamiya, Prog. Theor. Exp. Phys. **2012**, 02B001 (2012).

[19] J. K. Ahn et al. (KOTO Collaboration), Prog. Theor. Exp. Phys. **2017**, 021C01 (2017).

[20] K. Fuyuto, W.-S. Hou, and M. Kohda, Phys. Rev. Lett. **114**, 171802 (2015).

[21] K. Fuyuto, W.-S. Hou, and M. Kohda, Phys. Rev. D **93**, 054021 (2016).

[22] H. Takahashi et al., J. Radioanal. Nucl. Chem. **305**, 803 (2015).

[23] T. Shimogawa, Nucl. Instrum. Methods Phys. Res., Sect. A **623**, 585 (2010).

[24] K. Shiomi et al., Nucl. Instrum. Methods Phys. Res., Sect. A **664**, 264 (2012).

[25] T. Masuda et al., Prog. Theor. Exp. Phys. **2016**, 013C03 (2016).

[26] T. Matsumura, I. Kamiji, K. Nakagiri, H. Nanjo, T. Nomura, N. Sasao, T. Shinkawa, and K. Shiomi, Nucl. Instrum. Methods Phys. Res., Sect. A **885**, 91 (2018).

[27] M. Bogdan, J. Genat, and Y. Wah, in Proceedings of the 16th IEEE-NPSS Real Time Conference, Beijing, 2009 (2009), pp. 443–445, https://doi.org/10.1109/RTC.2009.5321611.

[28] M. Bogdan, J. Genat, and Y. Wah, in Proceedings of the 17th IEEE-NPSS Real Time Conference, Lisbon, 2010 (2010), pp. 1,2, https://doi.org/10.1109/RTC.2010.5750452.

[29] K. Shiomi, J. Phys. Conf. Ser. **800**, 012022 (2017).

[30] Y. Sugiyama et al., IEEE Trans. Nucl. Sci. **62**, 1115 (2015).

[31] S. Su et al., IEEE Trans. Nucl. Sci. **64**, 1338 (2017).

[32] S. Agostinelli et al., Nucl. Instrum. Methods Phys. Res., Sect. A **506**, 250 (2003).

[33] J. Allison et al., IEEE Trans. Nucl. Sci. **53**, 270 (2006).

[34] J. Allison et al., Nucl. Instrum. Methods Phys. Res., Sect. A **835**, 186 (2016).

[35] K. Nakagiri, J. Phys. Conf. Ser. **800**, 012025 (2017).

[36] K. Sato, Ph.D. thesis, Osaka University, 2015, http://osksn2.hep.sci.osaka-u.ac.jp/theses/doctor/2015/dt_sato.pdf.

[37] Y. Sugiyama, Ph.D. thesis, Osaka University, 2016, http://osksn2.hep.sci.osaka-u.ac.jp/theses/doctor/2016/dt_sugiyama.pdf.

[38] A. Hoecker et al., Proc. Sci. ACAT2007 (**2007**) 040.

[39] D. Naito et al., Prog. Theor. Exp. Phys. **2016**, 023C01 (2016).

[40] R. D. Cousins and V. L. Highland, Nucl. Instrum. Methods Phys. Res., Sect. A **320**, 331 (1992).

[41] M. Togawa, J. Phys. Conf. Ser. **800**, 012043 (2017).